CrystEngComm

Controllable Growth of Two-Dimensional Perovskite Microstructures

Journal:	*CrystEngComm*
Manuscript ID	CE-ART-07-2018-001087.R1
Article Type:	Paper
Date Submitted by the Author:	18-Aug-2018
Complete List of Authors:	Li, Dehui; University of California, Los Angeles, Chemistry and Biochemistry Fang, Chen; Huazhong University of Science and Technology Li, Junze; Huazhong University of Science and Technology Wang, Jun; Huazhong University of Science and Technology Chen, Rong; Huazhong University of Science and Technology Wang, Haizhen; New Mexico State University Lan, Shangui; Huazhong University of Science and Technology Xuan, Yining; Huazhong University of Science and Technology Luo, Hongmei; New Mexico State University, Fei, Peng; Huazhong University of Science and Technology, Optical and Electronic Information

Controllable Growth of Two-Dimensional Perovskite Microstructures

Chen Fang[1], Junze Li[1], Jun Wang[1], Rong Chen[1], Haizhen Wang[2], Shangui Lan[1], Yining Xuan[1], Hongmei Luo[2], Peng Fei[1] and Dehui Li[1, 3*]

[1]*School of Optical and Electronic Information, Huazhong University of Science and Technology, Wuhan, 430074, China;*

[2] *Department of Chemical and Materials Engineering, New Mexico State University, NM 88003, United States;*

[3]*Wuhan National Laboratory for Optoelectronics, Huazhong University of Science and Technology, Wuhan, 430074, China;*

*Correspondence to: Email: dehuili@hust.edu.cn.

Abstract

Two-dimensional (2D) Ruddlesden-Popper perovskites with large exciton binding energy and great environmental stability have recently attracted great attention for their promising potential optoelectronic applications. Controllable growth of 2D perovskites with desired shape would be critical for improving the performance of 2D perovskite based optoelectronic devices. However, the investigation on this is still in its infancy. Here we report on the controllable synthesis of 2D $(C_4H_9NH_3)_2PbI_4$ microstructures with butterfly shape, $(C_4H_9NH_3)_2(CH_3NH_3)Pb_2I_7$ and $(C_4H_9NH_3)_2PbI_4/(C_4H_9NH_3)_2(CH_3NH_3)Pb_2I_7$ microstructures with square shape by a solution-processed method. We have systematically investigated the influence of substrate, mass ratio and crystallization temperature on the morphology evolution of the as-synthesized 2D perovskite microstructures. Atomic force microscope (AFM) and optical microscope (OM) images show that the size and thickness of the resultant products are positively correlated with mass ratio and negatively correlated with crystallization temperature. X-ray diffraction (XRD) pattern, fluorescence imaging, temperature-dependent photoluminescence (PL) and absorption studies confirm the crystalline structures and optical properties of the as-synthesized regular shaped 2D perovskite microstructures. Our studies provide a simple method to controllably synthesize 2D

perovskite microstructures without using very toxic solvent and thus offer a platform to investigate the optical and charge transport properties of 2D perovskite materials for further designing new device architectures with enhanced performance.

1. Introduction

Organic-inorganic lead halide perovskites, especially $CH_3NH_3PbX_3$ (X=Cl, Br, I), have undergone an unprecedented progress in optoelectronic applications such as solar cells,[1,2] photodetectors,[3-6] lasers,[7,8] transistors and light-emitting devices.[9-14] Up to date, the power conversion efficiency of perovskite based solar cells has been increased rapidly to more than 22% within just a few years due to the strong light absorption,[10,15-21] long carrier diffusion length and modest carrier mobility of those perovskite materials within three-dimensional (3D) frameworks.[22-25]

However, 3D perovskites also have many drawbacks such as long-term instability against moisture, heat and light illumination, which prevent their further commercial applications.[2,26-30] One feasible solution to address the long-term stability issue of 3D perovskite is the two-dimensional (2D) Ruddlesden-Popper perovskites with large exciton binding energy and great environmental stability,[31-33] which thus have attracted extensive studies recently.[34-38] These 2D perovskites have the general chemical formula $R_2(A)_{n-1}MX_{3n+1}$ (where R is a long chain cation acting as a spacer, X is a halogen, M is a bivalent metal cation, A is an organic cation and n is an integer from 1 to ∞). The structure of 2D perovskite consists of layers of $[MX_6]^{4-}$ octahedra confined between the long chain organic molecules, forming a multi-quantum well structure.[39] Up to date, several methods have been proposed for the growth of specific morphology of $(C_4H_9NH_3)_2PbX_4$ and $(C_6H_5CH_2NH_3)_2PbX_4$ films while the controllable morphology of 2D

perovskite individual microstructure is in its infancy.[35,40-41] The controllable synthesis of 2D perovskite nanostructures with desired shape is critical for investigating the optical and charge transport properties of 2D perovskite materials for further designing new device architectures with enhanced performance due to their unique size and morphology dependent optical and electronic properties.[42] Furthermore, 2D perovskites with specially designed shape can improve the performance of 2D perovskite based optoelectronic devices and lay a foundation for future research on integrated optoelectronic device arrays. In addition, controllable growth of 2D perovskites makes it possible to fabricate individual microstructure device of 2D perovskite so that the basic optical and electronic parameters of 2D perovskites can be extracted for further optimizing the optoelectronic devices. Recently, butterfly shaped 2D $(C_4H_9NH_3)_2PbBr_4$ perovskite microstructures have been synthesized with controllable size by carefully selecting the solvent used.[38] Nevertheless, the very toxic unfavorable virulent reagent acetonitrile (ACN) has been used in order to achieve the high controllability of the resultant microstructures.

Here we report on the controllable growth of 2D $(C_4H_9NH_3)_2(CH_3NH_3)_{n-1}Pb_nI_{3n+1}$ with various shapes and sizes by tuning the mass ratio and crystalline temperature without using the very toxic ACN solution. We have not only successfully synthesized butterfly-shaped $(C_4H_9NH_3)_2PbI_4$ microstructures, but also obtained $(C_4H_9NH_3)_2(CH_3NH_3)Pb_2I_7$ and $(C_4H_9NH_3)_2PbI_4/(C_4H_9NH_3)_2(CH_3NH_3)Pb_2I_7$ square plates by rationally alternating the compositions of ingredients. Atomic force microscopy (AFM) and optical microscopy (OM) studies reveal how the crystal size and thickness of the resultant 2D perovskite microstructures correlate with the crystallization temperature and the mass ratio of perovskites dissolved in

n-dimethylformamide (DMF). XRD pattern, fluorescence imaging, temperature-dependent PL and absorption spectroscopy confirm the excellent crystalline quality and optical properties of the resultant regular shaped 2D perovskite microstructures.

2. Experimental section

2.1 Synthesis of Methylammonium chloride (MACl)/n-butylammonium iodide (BAI): For the synthesis of MACl, aqueous methylamine (MA, 40 wt.% in water) was dropped into hydrochloric acid (HCl, 32 wt.% in water) solution with a molar ratio of 1:1 at 0 °C accompanied by stirring for two hours. The mixed solution was washed by diethyl ether three times after evaporated at 60 °C and then dried at 70 °C for 12 hours to obtain the MACl powder. As for BAI solution, the same procedure was adopted except that the MA and HCl solution was replaced by n-butylamine (BA) and hydriodic acid (HI) solution respectively and the stirring time was prolonged to four hours.

2.2 Synthesis of 2D perovskite sources: The perovskites were synthesized using a previously reported method.[33,43,44] 0.5 g PbO powder, 0.5 ml hypophosphorous acid (H_3PO_2, 50 wt.% in water) solution and 3 ml hydriodic acid (HI, 57 wt.% in water) solution were mixed in a flask and heated to 140 °C with magnetic stirring. Then 2.5 mmol BAI solution was added to the mixture in order to obtain $(BA)_2PbI_4$ plates while 0.169 g MACl and 1.75 mmol BAI solution were added to get $(BA)_2(MA)Pb_2I_7$ plates. For the synthesis of $(BA)_2PbI_4/(BA)_2(MA)Pb_2I_7$ square plates, 1.21 mmol BAI solution was added to the mixed solution first and kept heating for 5 mins and then 0.169 g MACl was added to obtain the plates. After 10 minutes, the stirring was stopped and the solution was left to cool to room temperature naturally. After being kept static overnight, the as-prepared perovskite plates were dried at 130 °C for 1 hour and dissolved in DMF to form the solution at a specific mass ratio for further synthesizing 2D perovskite microstructures with

regular shape.

2.3 Synthesis of regular shaped 2D perovskite microstructures: For the synthesis of $(BA)_2PbI_4$ butterflies, the pre-cleaned glass or SiO_2/Si substrates were treated by a plasma cleaner (PT-2S) for 180 s, and the as-prepared perovskite precursor solution in DMF (the mass ratio of perovskites: 4.5%, 6%, 8.25%, 12.5%, 15% and 25%) was spin-coated onto the substrates at 1000 rpm for 10 s followed by 4000 rpm for 20 s before it was dried at a series of temperatures varied from 25 °C to 130 °C. As for $(BA)_2(MA)Pb_2I_7$ and $(BA)_2PbI_4$/$(BA)_2(MA)Pb_2I_7$ square microplates, the similar procedure was adopted except that the spin-coating speed was changed to 4000 rpm for 40 s.

2.4 Characterizations: Ultraviolet-vis absorbance spectra were performed on a Lambda 35 Ultraviolet-vis spectrophotometer. The photoluminescence (PL) measurements were carried out on a home-built microRaman spectrometer (Horiba JY iHR550) in a backscattering configuration collected by the spectrometer excited by a 405-nm laser with a power of 1 μW. The temperature-dependent PL measurements were performed in the same configuration equipped with a liquid helium continuous flow cryostat and the temperature was controlled by a temperature controller (Lake Shore Model 336). XRD patterns were performed on a Bruker D2 PHPSER (Cu Kα λ=0.1542 nm, Nickel filter, 25 kV, 40 mA). The fluorescence images were acquired through a Olympus BX51 microscope excited by a 488-nm LED. The scanning electron microscopy (SEM) images were taken on a TESCAN microscopy (TESCAN SB). Thicknesses of the microstructures were confirmed by atom force microscope (AFM, Bruker Dimension Edge) and optical images were acquired by an optical microscope (OM, Mshot-MJ30).

3. Results and Discussion

The schematic illustrations of the synthesis of $(BA)_2(MA)_{n-1}Pb_nI_{3n+1}$ microstructures are

presented in Fig. 1a. First, the as-synthesized perovskite crystals were dissolved in DMF solution at a specific mass ratio. Then the mixed solution was spin-coated onto the substrates followed by annealed at an appropriate temperature to form regular shapes. Fig. 1b shows the schematics of the crystal structures of $(BA)_2PbI_4$ (denoted as n=1), $(BA)_2(MA)Pb_2I_7$ (denoted as n=2) and $(BA)_2PbI_4/(BA)_2(MA)Pb_2I_7$ (denoted as n=1-n=2) perovskites, which illuminate that the basic multi-quantum well structure of these 2D perovskites consists of layers of $[PbI_6]^{4-}$ octahedra sandwiched between the long chain organic molecules.[33,37] The 2D perovskite crystal is then formed by stacking the $(BA)_2(MA)_{n-1}Pb_nI_{3n+1}$ layers along specific axis via weak Van der Waals forces.

Fig. 2a-c show the OM images of $(BA)_2(MA)_{n-1}Pb_nI_{3n+1}$ microstructures for n=1, n=2 and n=1-n=2. The corresponding SEM images in Fig. 2d-f indicate their relative smooth surface and regular shape. Fig. 2g-i show the AFM images of the as-synthesized microstructures. As seen in Fig. 2a, the AFM image confirms the relatively smooth surface of $(BA)_2PbI_4$ butterflies with a thickness of 78 nm while a small number of randomly irregular perovskites are found around the microstructure. Fig. 2b shows that the $(BA)_2(MA)Pb_2I_7$ plates also possess smooth surface with regular square shape. Fig. 2b and Fig. 2c show the striking color difference between $(BA)_2(MA)Pb_2I_7$ and $(BA)_2PbI_4/(BA)_2(MA)Pb_2I_7$ square plates. As seen in Fig. 2c, the dark shadow inside the square plate shares the same butterfly shape as $(BA)_2PbI_4$ compound. We then inferred a possible situation that the $(BA)_2PbI_4$ butterflies crystallized first and subsequently the $(BA)_2(MA)Pb_2I_7$ compound grew surrounding the $(BA)_2PbI_4$ compound, resulting in the $(BA)_2PbI_4/(BA)_2(MA)Pb_2I_7$ heterojunctions. Powder X-ray diffraction (XRD) patterns (Fig. 2d) indicate that the diffraction peaks of as-synthesized n=1 and n=2 2D perovskite compounds agree

well with previously reported 2D perovskite crystals.[32,33,46] For the n=1-n=2 square plates, both the n=1 and n=2 perovskite phases appear, confirming the existence of the n=1 and n=2 phase.

Generally, the mass ratio of perovskites in DMF and the crystallization temperature are the two critical factors to determine the size and thickness of the resultant products.[40] As seen in Fig. 3, OM images of the as-synthesized $(BA)_2PbI_4$ butterflies spin-coated on Si substrates show that the morphology is closely related to the mass ratio. At a low mass ratio of 4.5%, small size perovskite butterflies with not very regular shapes are acquired owing to insufficient solute source supplied during spin-coating process (Fig. 3a). As the mass ratio increases from 6% to 25%, the size and thickness of the butterflies increase simultaneously and the shapes become more regular due to the increase of the available precursor source (Fig. 3b-e). However, the perovskite butterflies will be stacked together when mass ratio is too high. Indeed, the optimal mass ratio to obtain the butterfly-shaped $(BA)_2PbI_4$ microstructures is around 8.25%. Fig. 3f summarizes how the size and thickness of $(BA)_2PbI_4$ butterflies evolve with respect to the mass ratio, which indicates that both the size and thickness of the as-growth $(BA)_2PbI_4$ butterflies continuously increase with the increase of the mass ratio.

Subsequently, we found the perovskite morphology could also be grown on glass substrate and the similar experimental result was achieved as that on Si substrate. Furthermore, we studied the influence of the crystallization temperature on the morphology evolution of $(BA)_2PbI_4$ at a fixed mass ratio of 8.25%. As shown in Fig. S1, the size and thickness of the final products are negatively correlated with crystallization temperature. When the substrates with spin-coated perovskite solution are baked at room temperature, $(BA)_2PbI_4$ butterflies with large size which are surrounded by irregular shaped perovskites have formed (Fig. S1a). As the temperature increases

from room temperature to 70°C, the size of butterflies continuously decreases and the nucleation density gradually increases owing to the fast evaporation rate.[40] Meanwhile, the unshaped perovskite structures decrease since the higher bake temperature can help improve the crystallinity (Fig. S1a-c). When further raising the crystallization temperature, the perovskite butterflies become smaller and thinner and at the same time they begin to crumble (Fig. S1d). The butterflies are almost all turned into broken fragments when the temperature reaches to 130°C (Fig. S1e). The size and thickness of $(BA)_2PbI_4$ with respect to the crystallization temperature are summarized in Fig. S1f. Indeed, the temperature of 70°C was found to be optimum temperature to acquire the butterfly-shape perovskites with the best surface morphology and suitable size and thickness.

We further investigated the morphology evolution of $(BA)_2(MA)Pb_2I_7$ and $(BA)_2PbI_4/(BA)_2(MA)Pb_2I_7$ square plates. As shown in Fig. 4 and Fig. S2, OM images reveal the size and thickness of $BA)_2(MA)Pb_2I_7$ and $(BA)_2PbI_4/(BA)_2(MA)Pb_2I_7$ square plates follow the similar variation trend as that of $(BA)_2PbI_4$ with the change of the mass ratio (Fig. 4f, Fig. S2f). For $(BA)_2(MA)Pb_2I_7$, the plates are more disperse and coexist with less unshaped matter compared to $(BA)_2PbI_4$ at low mass ratios (Fig. 4a-c), which is mainly due to the more regular crystal morphology. However, further increasing concentration will result in distorted square plates and introduce a small number of randomly irregular shaped perovskites (Fig. 4d, e). For $(BA)_2PbI_4/(BA)_2(MA)Pb_2I_7$ microstructures, the optimal square plates are acquired when the mass ratio is lower than 12.5% (Fig. S2a-c). The perovskite plates will coalesce together at higher concentrations (Fig. S2d, e). It's worth noting that the n=1-n=2 square plates are as dense as n=1 microstructures and the shape is not as regular as n=2 plates. This can to some extent support our

previous assumption that the $(BA)_2PbI_4$ compound crystallizes ahead of the $(BA)_2(MA)Pb_2I_7$ compound and the $(BA)_2PbI_4$ butterflies become the nucleation sites for the surrounding $(BA)_2(MA)Pb_2I_7$ compound to grow.

To sum up, both the mass ratio and the temperature play important roles in the crystal size and thickness of the as-growth 2D microstructures. The temperature affects the nucleation density and growth rate, while the mass ratio of the precursor determines the available precursor source for the microstructure to be grown. The higher the crystallization temperature is, the faster the nucleation and growth are, leading to a smaller size of the microstructure at a higher temperature due to the faster evaporation rate. In terms of the mass ratio, the higher the mass ratio is, the larger the size of the resultant microstructures is, due to a larger amount of the available precursor source. Both the two factors can affect the final morphology but from different aspects.

To explore the optical properties of the synthesized microstructures, fluorescence imaging, PL and absorption measurement were carried out. Fig 5a-c display the fluorescence images of as-synthesized $(C_4H_9NH_3)_2(CH_3NH_3)_{n-1}Pb_nI_{3n+1}$ microstructures. N=1 butterflies exhibit the strongest fluorescence owing to the strongest quantum limiting effects of n=1 compound while n=1-n=2 microplates show the weakest emission because of the type II band alignment between n=1 and n=2 compounds which can result in the separation of the photogenerated electrons and holes.[44,45] Fig. 5d shows the PL spectra of n=1, n=2 and n=1-n=2 2D perovskite compounds. The peak of n=2 has a redshift relative to the peak of n=1, which is owing to the weaker quantum confinement effect in n=2 compounds. 32.[33] The size and morphology can also have slightly influence on the PL spectra. In terms of the size effect, the quantum confinement can be neglected as the size is much larger than the bulk exciton Bohr radius as in our case. But the surface effect

might induce the slight shift of the emission peak and the decrease of the emission intensity due to the surface depletion electric field.[46] Fig. 5e shows the absorbance spectra of the as-synthesized perovskites. In addition to the absorption edge from their respective band edge,[33,47] a small peak at 610 nm appears in the spectra of both $(BA)_2(MA)Pb_2I_7$ and $(BA)_2PbI_4/(BA)_2(MA)Pb_2I_7$ square plates, which might be due to the presence of small inclusions of $(BA)_2(MA)_2Pb_3I_{10}$.

To further check the crystalline quality of the as-synthesized 2D perovskite microstructures, we have also performed the temperature-dependent PL measurement. As shown in Fig. 6a-c, the absence of emission peak from impurities and narrow peak width indicate the high crystallinity and purity of these regular shape 2D perovskites.[32,33] The peak position of $(BA)_2PbI_4$ butterflies shifts from 487 nm to 494 nm as the temperature increases from 77 K to 260 K, then jumps to 520 nm around 280 k due to an orthorhombic-to-orthorhombic phase transition, consistent with previous studies (Figure 6d).[48,49] As for $(BA)_2(MA)Pb_2I_7$ square plates shown in Fig. 6e, the peak position shows a blue shift from 77 K to 140 K and then a red shift when the temperature is higher than 140 K, agreeing well with that of solution-processed $(BA)_2(MA)Pb_2I_7$ plates. As expected, PL spectra of $(BA)_2PbI_4/(BA)_2(MA)Pb_2I_7$ square plates contain emission peaks from both n=1 and n=2 peaks at all temperature as shown in Fig. 6c and f. Importantly, as the temperature increases, those two peak positions in n=1-n=2 follows exactly same trend as that of n=1 and n=2, respectively (Fig. 6f), which can further confirm the high crystalline quality of the as-synthesized structures.

Finally, we found that the morphology of the as-synthesized microstructures strongly depends on the rotation speed during spin-coating process. When the solution was spin-coated on the pretreated substrate, a thin solution layer was evenly distributed on the hydrophilic surface to

allow the nucleation of crystal seeds.[50] Subsequently, the crystal seeds became larger and turned into specific microstructures with the process of evaporation. If the rotation speed is too slow, the perovskite solution layer would be relatively thick. Therefore, the redundant solution will drive the formed microstructures continue to grow and finally aggregate into a thick film. On the contrary, when the rotation speed is too fast, the perovskite solution layer should be relatively thin leading to the cease of the further growth of crystal seeds. As a result, a large number of irregular perovskites appear. The perovskite butterflies or square plates can be acquired only if the rotation speed is appropriately selected. The suitable thickness of solution layer can provide enough precursor source to exactly crystallize into isolate shapes and prevent them from aggregating into a film. The optimal rotation speed is 1000 rpm for 10s followed by 4000 rpm for 20s to $(BA)_2PbI_4$ butterflies and 4000 rpm for 40s to $(BA)_2(MA)Pb_2I_7$ and $(BA)_2PbI_4$/$(BA)_2(MA)Pb_2I_7$ square plates.

4. Conclusions

In summary, we report on the synthesis of 2D $(BA)_2PbI_4$ butterflies, $(BA)_2(MA)Pb_2I_7$ and $(BA)_2PbI_4$/$(BA)_2(MA)Pb_2I_7$ square plates by a solution-processed method. We have systematically investigated the factors that critically affect the morphology of the as-synthesized 2D perovskites. Our studies reveal that the size and thickness of the resultant products were positively correlated with mass ratio and negatively correlated with crystallization temperature. XRD, fluorescence imaging, PL and absorption studies indicate the good crystalline quality and excellent optical properties. Our work provides a simple method to controllably synthesize 2D perovskite microstructures without using very toxic solvent and offer a platform to investigate the optical and charge transport properties of 2D perovskite materials for further designing new device architectures with enhanced performance.

Conflicts of interest

There are no conflicts to declare.

Acknowledgements

D. L. acknowledges the support from NSFC (61674060) and the Fundamental Research Funds for the Central Universities, HUST (2017KFYXJJ030, 2017KFXKJC003, 2017KFXKJC003, 2018KFYXKJC016) and National Young 1000 Talent Plan of China; H. L. thanks the support from New Mexico EPSCoR with NSF-1301346. We thank Hong Cheng engineer in the Analytical and Testing Center of Huazhong University of Science and Technology for the support in PL measurement and thank the Center of Micro-Fabrication of WNLO for the support in device fabrication.

References

1 W. -J. Yin, J. -H. Yang, J. Kang, Y. Yan and S. -H. Wei, J. Mater. Chem. A, 2015, 3, 8926.

2 G. D. Niu, X. D. Guo and L. D. Wang, J. Mater. Chem. A, 2015, 3, 8970.

3 S. Shrestha, R. Fischer, G. J. Matt, P. Feldner, T. Michel, A. Osvet, I. Levchuk, B. Merle, S. Golkar, H. Chen, S. F. Tedde, O. Schmidt, R. Hock, M. Rührig, M. Göken, W. Heiss, G. Anton and C. J. Brabec, Nat. Photon., 2017, 11, 436.

4 H. Wei, D. DeSantis, W. Wei, Y. Deng, D. Guo, T. J. Savenije, L. Cao and J. Huang, Nat. Mater., 2017, 16, 826.

5 W. Lee, J. Lee, H. Yun, J. Kim, J. Park, C. Choi, D. C. Kim, H. Seo, H. Lee, J. W. Yu, W. B. Lee and D. H. Kim, Adv. Mater., 2017, 29, 1702902.

6 J. Li, S. H. Yuan, G. Q. Tang, G. J. Li, D. Liu, J. Li, X. H. Hu, Y. C. Liu, J. B. Li, Z. Yang, S. Z. F. Liu, Z. K. Liu, F. Gao and F. Yan, ACS Appl. Mat. Interfaces, 2017, 9, 42779.

7 G. Xing, N. Mathews, S. S. Lim, N. Yantara, X. Liu, D. Sabba, M. Grätzel, S. Mhaisalkar and T. C. Sum, Nat. Mater., 2014, 13, 476.

8 X. Li, Y. Wang, H. Sun and H. Zeng, Adv. Mater., 2017, 29, 1701185.

9 N. Wang, L. Cheng, R. Ge, S. Zhang, Y. F. Miao, W. Zou, C. Yi, Y. Sun, Y. Cao, R. Yang, Y. H. Wei,

Q. Guo, Y. Ke, M. T. Yu, Y. Z. Jin, Y. Liu, Q. Q. Ding, D. W. Di, L. Yang, G. C. Xing, H. Tian, C. H. Jin, F. Gao, R. H. Friend, J. P. Wang and W. Huang, Nat. Photon., 2016, 10, 699.

10 Z. G. Xiao, R. A. Kerner, L. Zhao, N. L. Tran, K. M. Lee, T. -W. Koh, G. D. Scholes and B. P. Rand, Nat. Photon., 2017, 11, 108.

11 L. N. Quan, Y. B. Zhao, F. P. Garcia de Arquer, R. Sabatini, G. Walters, O. Voznyy, R. Comin, Y. Y. Li, J. Z. Fan, H. R. Tan, J. Pan, M. J. Yuan, O. M. Bakr, Z. H. Lu, D. H. Kim and E. H. Sargent, Nano Lett., 2017, 17, 3701.

12 Z. Yuan, C. K. Zhou, Y. Tian, Y. Shu, J. Messier, J. C. Wang, L. J. van de Burgt, K. Kountouriotis, Y. Xin, E. Holt, K. Schanze, R. Clark, T. Siegrist and B. Ma, Nat. Commun., 2017, 8, 14051

13 D. H. Li, H. C. Cheng, Y. L. Wang, Z. P. Zhao, G. M. Wang, H. Wu, Q. Y. He, Y. Huang and X. F. Duan, Adv. Mater., 2017, 29, 1601959.

14 D. J. Yu, F. Cao, Y. J. Gao, Y. H. Xiong and H. B. Zeng, Adv. Funct. Mater., 2018, 28, 1800248.

15 M. M. Lee, J. Teuscher, T. Miyasaka, T. N. Murakami and H. J. Snaith, Science, 2012, 338, 643.

16 M. A. Green, A. Ho-Baillie and H. J. Snaith, Nat. Photon., 2014, 8, 506.

17 W. S. Yang, J. H. Noh, N. J. Jeon, Y. C. Kim, S. Ryu, J. Seo and S. I. Seok, Science, 2015, 348, 1234.

18 M. Saliba, T. Matsui, K. Domanski, J. -Y. Seo, A. Ummadisingu, S. M. Zakeeruddin, J. -P. Correa-Baena, W. R. Tress, A. Abate, A. Hagfeldt and M. Grätzel, Science, 2016, 354, 206.

19 W. Nie, H. Tsai, R. Asadpour, J. -C. Blancon, A. J. Neukirch, G. Gupta, J. J. Crochet, M. Chhowalla, S. Tretiak, M. A. Alam, H. -L. Wang and A. D. Mohite, Science, 2015, 347, 522.

20 N. Ahn, D. Y. Son, I. H. Jang, S. M. Kang, M. Choi and N. G. Park, J. Am. Chem. Soc., 2015, 137, 8696.

21 J. S. Shaikh, N. S. Shaikh, A. D. Sheikh, S. S. Mali, A. J. Kale, P. Kanjanaboos, C. K. Hong, J. H. Kim and P. S. Patil, Mater.& Des., 2017, 136, 54.

22 D. Shi, V. Adinolfi, R. Comin, M. Yuan, E. Alarousu, A. Buin, Y. Chen, S. Hoogland, A. Rothenberger, K. Katsiev, Y. Losovyj, X. Zhang, P. A. Dowben, O. F. Mohammed, E. H. Sargent and O. M. Bakr, Science, 2015, 347, 519.

23 M. B. Johnston and L. M. Herz, Acc. Chem. Res., 2016, 49, 146.

24 T. M. Brenner, D. A. Egger, L. Kronik, G. Hodes and D. Cahen, Nat. Rev. Mater., 2016, 1, 15007.

25 J. S. Huang, Y. B. Yuan, Y. C. Shao and Y. F. Yan, Nat. Rev. Mater., 2017, 2, 17042.

26 M. H. Kumar, S. Dharani, W. L. Leong, P. P. Boix, R. R. Prabhakar, T. Baikie, C. Shi, H. Ding, R. Ramesh, M. Asta, M. Graetzel, S. G. Mhaisalkar and N. Mathews, Adv. Mater., 2014, 26, 7122.

27 C. -H. Chiang, M. K. Nazeeruddin, M. Grätzel and C. -G. Wu, Energy Environ. Sci., 2017, 10, 808.

28 J. B. Huang, S. Q. Tan, P. D. Lund and H. P. Zhou, Energy Environ. Sci., 2017, 10, 2284.

29 X. Li, M. I. Dar, C. Y. Yi, J. S. Luo, M. Tschumi, S. M. Zakeeruddin, M. K. Nazeeruddin, H. Han and M. Gratzel, Nat. Chem., 2015, 7, 703.

30 Y. G. Rong, L. F. Liu, A. Y. Mei, X. Li and H. W. Han, Adv. Energy Mater., 2015, 5, 1501066.

31 I. C. Smith, E. T. Hoke, D. Solis-Ibarra, M. D. McGehee and H. I. Karunadasa, Angew. Chem., 2014, 53, 11232.

32 D. H. Cao, C. C. Stoumpos, O. K. Farha, J. T. Hupp and M. G. Kanatzidis, J. Am. Chem. Soc., 2015, 137, 7843.

33 C. C. Stoumpos, D. H. Cao, D. J. Clark, J. Young, J. M. Rondinelli, J. I. Jang, J. T. Hupp and M. G. Kanatzidis, Chem. Mater., 2016, 28, 2852.

34 L. Pedesseau, D. Sapori, B. Traore, R. Robles, H. H. Fang, M. A. Loi, H. Tsai, W. Nie, J. C. Blancon, A. Neukirch, S. Tretiak, A. D. Mohite, C. Katan, J. Even and M. Kepenekian, ACS Nano, 2016, 10, 9776.

35 L. T. Dou, A. B. Wong, Y. Yu, M. L. Lai, N. Kornienko, S. W. Eaton, A. Fu, C. G. Bischak, J. Ma, T. Ding, N. S. Ginsberg, L. -W. Wang, A. P. Alivisatos and P. Yang, Science, 2015, 349, 1518.

36 H. Tsai, W. Nie, J. C. Blancon, C. C. Stoumpos, R. Asadpour, B. Harutyunyan, A. J. Neukirch, R. Verduzco, J. J. Crochet, S. Tretiak, L. Pedesseau, J. Even, M. A. Alam, G. Gupta, J. Lou, P. M. Ajayan, M. J. Bedzyk and M. G. Kanatzidis, Nature, 2016, 536, 312.

37 Y. N. Chen, Y. Sun, J. J. Peng, J. H. Tang, K. B. Zheng and Z. Q. Liang, Adv. Mater., 2017, 30, 1703487.

38 Z. Y. Chen and J. Lin, CrystEngComm, 2010, 12, 2646.

39 X. Hong, T. Ishihara and A. V. Nurmikko, Phys. Rev. B, 1992, 45, 6961.

40 J. N. Chen, L. Gan, F. W. Zhuge, H. Q. Li, J. Z. Song, H. B. Zeng and T. Y. Zhai, Angew. Chem., 2017, 129, 2430.

41 D. W. Ma and Y. D. He, J. Alloy Compd., 2017, 696, 1213.

42 C. M. M. Soe, W. Nie, C. C. Stoumpos, H. Tsai, J. -C. Blancon, F. Liu, J. Even, T. J. Marks, A. D. Mohite and M. G. Kanatzidis, Adv. Energy Mater., 2017, 8, 1700979.

43 C. C. Stoumpos, C. M. M. Soe, H. Tsai, W. Nie, J. -C. Blancon, D. H. Cao, F. Liu, B. Traoré, C. Katan, J. Even, A. D. Mohite and M. G. Kanatzidis, Chem., 2017, 2, 427.

44 J. Wang, J. Z. Li, Q. H. Tan, L. Li, J. B. Zhang, J. F. Zang, P. H. Tan, J. Zhang and D. H. Li, J. Phys. Chem. Lett., 2017, 8, 6211.

45 J. Z. Li, J. Wang, Y. J. Zhang, H. Z. Wang, G. M. Lin, X. Xiong, W. H. Zhou, H. M. Luo and D. H. Li, 2D Mater., 2018, 5, 021001.

46 D. H. Li, J. Zhang and Q. H. Xiong, ACS Nano, 2012, 6, 5283.

47 J. -C. Blancon, H. Tsai, W. Nie, C. C. Stoumpos, L. Pedesseau, C. Katan, M. Kepenekian, C. M. M. Soe, K. Appavoo, M. Y. Sfeir, S. Tretiak, P. M. Ajayan, M. G. Kanatzidis, J. Even, J. J. Crochet and A. D. Mohite, Science, 2017, 355, 1288-1292.

48 T. Ishihara, J. Takahashi and T. Goto, Phys. Rev. B, 1990, 42, 11099.

49 L. Ni, U. Huynh, A. Cheminal, T. H. Thomas, R. Shivanna, T. F. Hinrichsen, S. Ahmad, A. Sadhanala and A. Rao, ACS Nano, 2017, 11, 10834.

50 G. M. Wang, D. H. Li, H. C. Cheng, Y. J. Li, C. Y. Chen, A. X. Yin, Z. P. Zhao, Z. Y. Lin, H. Wu, Q. Y. He, M. N. Ding, Y. Liu, Y. Huang and X. F. Duan, Sci. Adv., 2015, 1, e1500613.

Figures

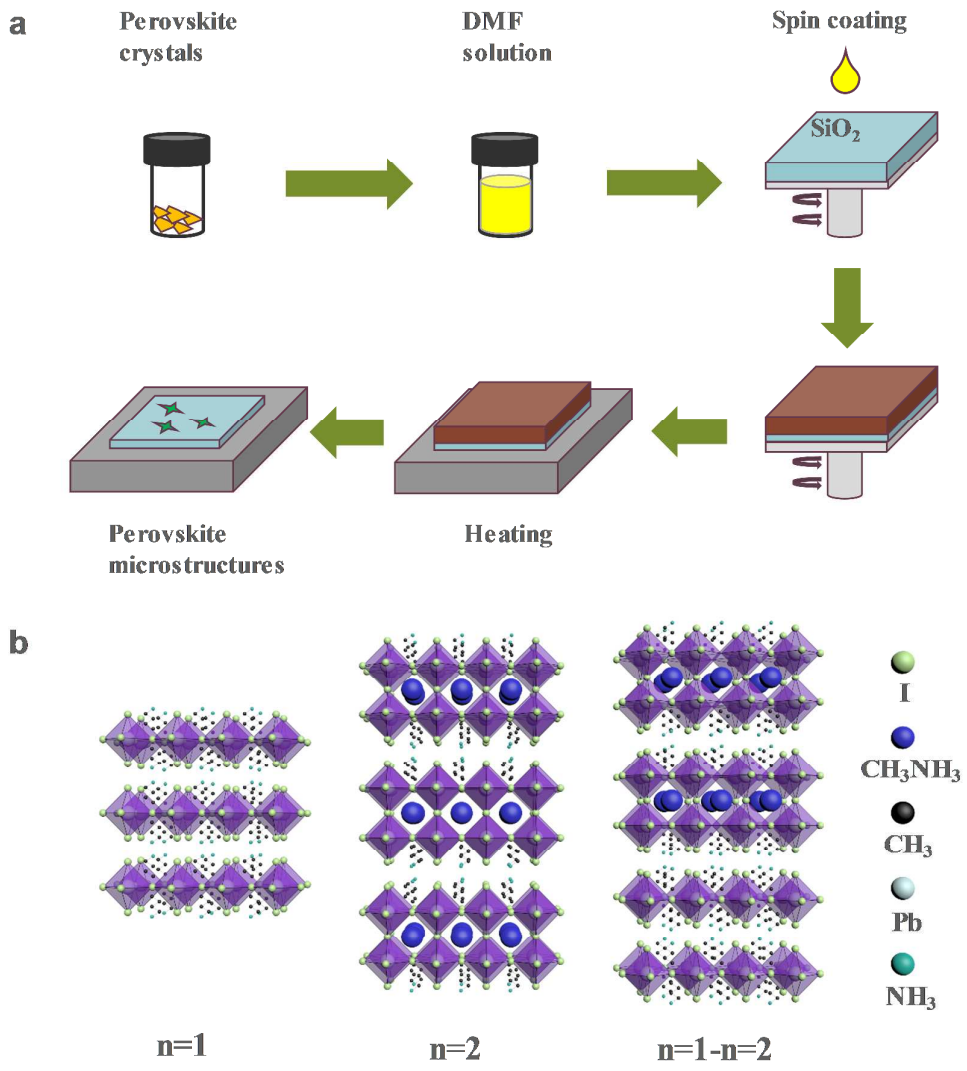

Fig. 1 (a) Stages in the synthesis of 2D perovskite $(BA)_2(MA)_{n-1}Pb_nI_{3n+1}$ microstructures by a solution-processed method. (b) The schematic illustrations of crystal structure of the 2D perovskite microstructures for n=1, n=2 and n=1-n=2 compound.

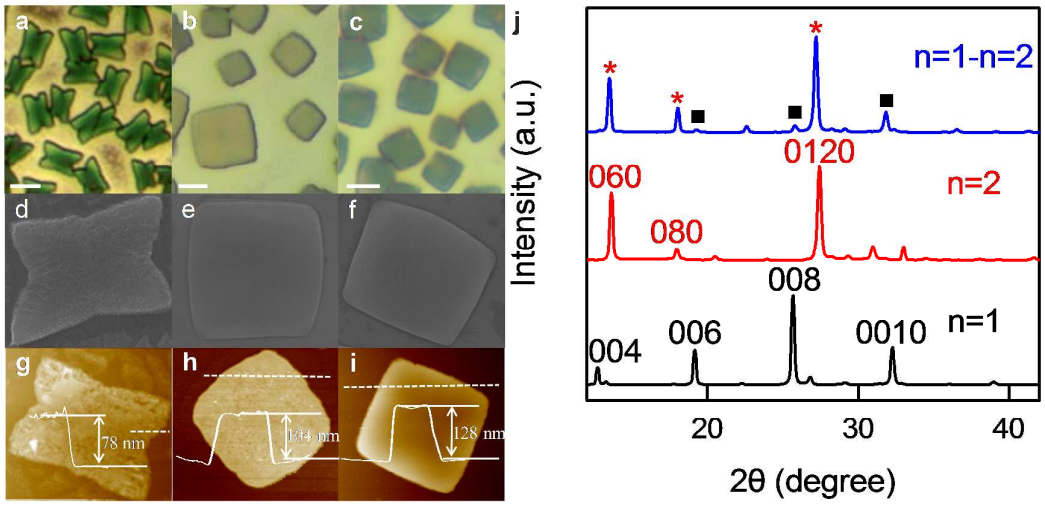

Fig. 2 (a-c) OM, (d-f) SEM and (g-i) AFM images of as-synthesized $(BA)_2(MA)_{n-1}Pb_nI_{3n+1}$ microstructures for n=1, n=2 and n=1-n=2 at mass ratios of 8.25%, 15% and 8.25%, respectively with the crystallization temperature of 70°C. The scale bar is 5 μm. (j) XRD of as-synthesized $(BA)_2(MA)_{n-1}Pb_nI_{3n+1}$ microstructures for n=1, n=2 and n=1-n=2 with main peaks indexed. Red stars: phase belongs to n=2 perovskite; Black squares: phase belongs to n=1 perovskite.

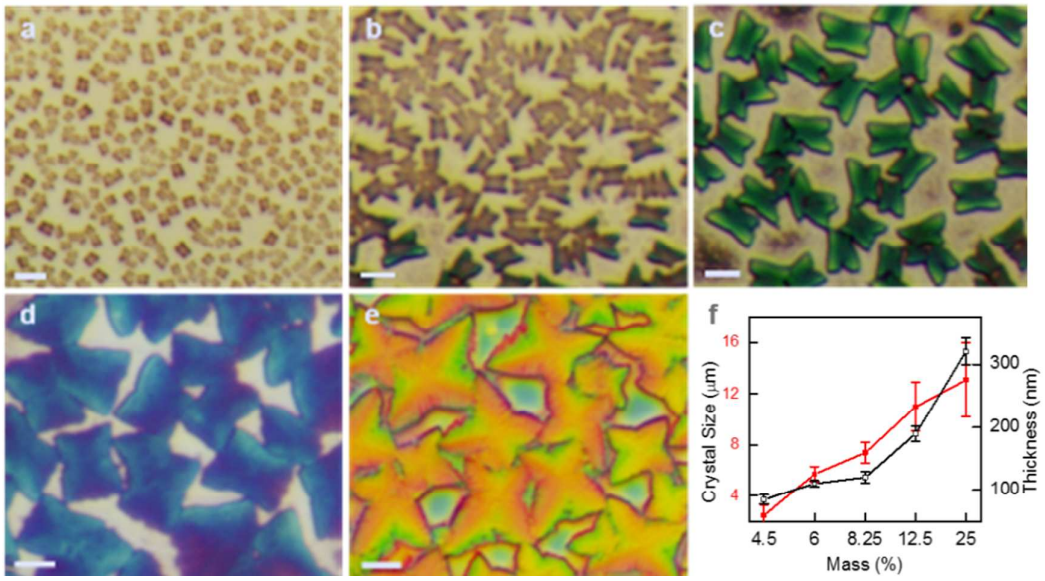

Fig. 3 OM images of $(BA)_2PbI_4$ butterflies grown on Si substrate at mass ratios of (a) 4.5%, (b) 6%, (c) 8.25%, (d) 12.5% and (e) 25% with the crystallization temperature of 70°C. The scale bar is 5 μm. (f) Plots of crystal size and thickness of $(BA)_2PbI_4$ butterflies against the perovskite mass ratio in DMF.

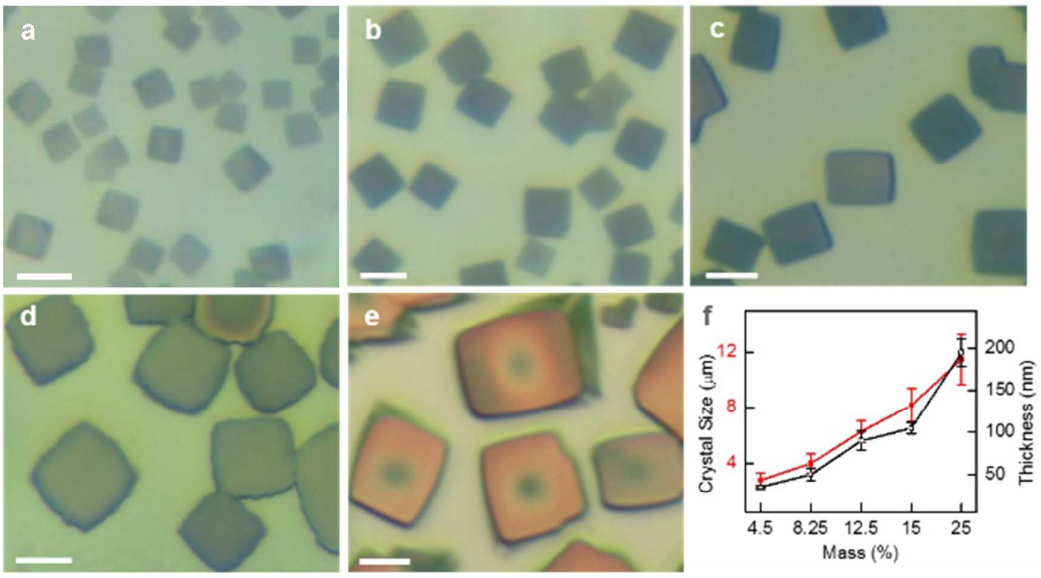

Fig. 4 OM images of $(BA)_2(MA)Pb_2I_7$ square plates grown on Si substrate at mass ratios of (a) 4.5%, (b) 8.25%, (c) 12.5%, (d) 15% and (e) 25% with the crystallization temperature of 70°C. The scale bar is 5 μm. (f) Plots of crystal size and thickness of $(BA)_2(MA)Pb_2I_7$ square plates with respect to the perovskite mass ratio in DMF.

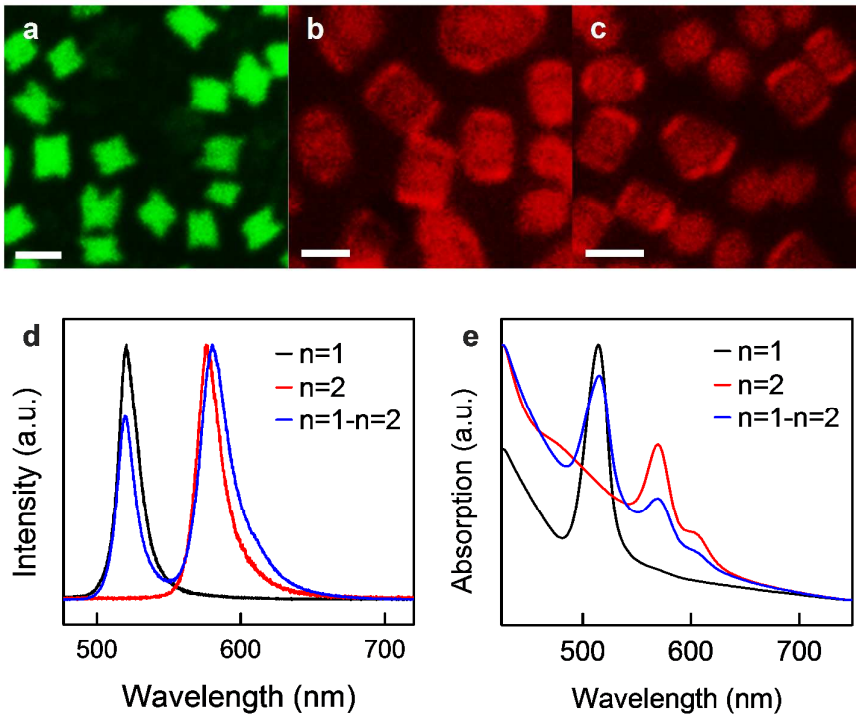

Fig. 5 (a-c) Fluorescence images of as-synthesized $(BA)_2(MA)_{n-1}Pb_nI_{3n+1}$ microstructures for n=1, n=2 and n=1-n=2 at mass ratios of 8.25%, 15% and 8.25%, respectively with the crystallization temperature of 70°C. The scale bar is 5 μm. (d) PL spectra and (e) absorption spectra of as-grown $(BA)_2(MA)_{n-1}Pb_nI_{3n+1}$ microstructures for n=1, n=2 and n=1-n=2.

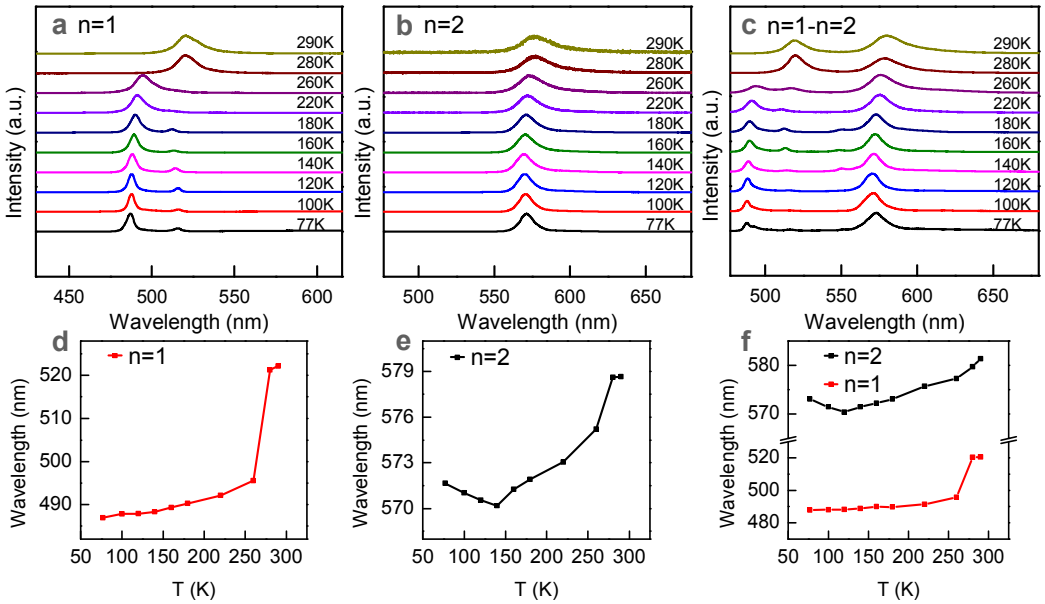

Fig. 6 (a-c) Temperature-dependent PL spectra and (d-f) their corresponding PL peak position of as-synthesized $(BA)_2(MA)_{n-1}Pb_nI_{3n+1}$ microstructures for n=1, n=2 and n=1-n=2 at mass ratios of 8.25%, 15% and 8.25%, respectively with the crystallization temperature of 70°C.

TOC

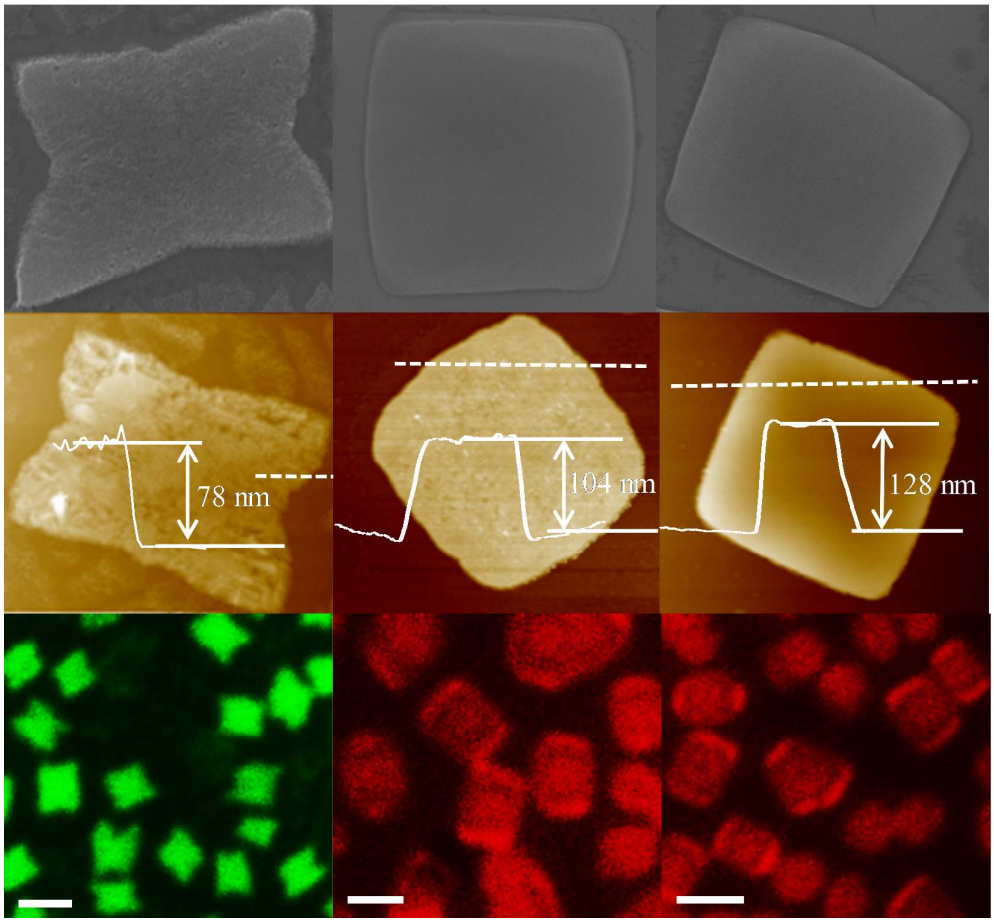

Controllable synthesis of 2D $(C_4H_9NH_3)_2(CH_3NH_3)_{n-1}Pb_nI_{3n+1}$ microstructures with various shapes and sizes for functional optoelectronics.